Dielectric diffuseness and conductivity behavior of Ba$_{1-x}$CuxTi$_{1-x}$(AlK)$_x$O$_3$ nanoceramics prepared by chemical route

Prasanta Dhak[1, 2,3*], **A. Kundu**[4], **K. Pramanik**[3], **P. Pramanik**[2], **D. Dhak**[5*]

[1]*National Creative Research Initiative Center for Spin Dynamics and Spin-Wave Devices and Research Institute of Advanced Materials, Department of Materials Science and Engineering, Seoul National University, Seoul 151-744, Republic of Korea*
[2]*Department of Chemistry, Indian Institute of Technology Kharagpur, Kharagpur 721302, India*
[3]*Department of Chemistry, Jadavpur University, Kolkata 700032, India*
[4]*Department of Biological Sciences, Presidency University, Kolkata 700073, India*
[5]*Department of Chemistry, Sidho-Kanho-Birsha University, Purulia 723101, India*

[*]Corresponding author. E-mail: pdhak_chem@yahoo.com; debasisdhak@yahoo.co.in

ABSTRACT

Small amounts of Cu and Al-K substitution on the A and B site of BaTiO$_3$, respectively resulting a solid solution of the type Ba$_{1-x}$Cu$_x$Ti$_{1-x}$(AlK)$_x$O$_3$ (BCTAK) [x = 0.05, 0.10, 0.15, 0.20] have been investigated. The compositions have been prepared in the nanocrystalline range by chemical route. X-ray diffraction revealed the tetragonal (P4/mmm) phase. Average crystallite size and particle size were found to be in the range between 25 nm and 35 nm which were analyzed through X-ray diffraction and transmission electron microscopy respectively. A dielectric study of these compounds as a function of temperature suggested that with increasing substitution concentration the dielectric constant decreased and the Curie temperature shifted towards the lower temperature side. Discontinuous grain growth accompanied with excellent dielectric diffuseness was found with increasing concentration of substitution. The dielectric diffuseness γ was found to be maximum to 1.91 at the substitution of BCTAK *x* = 0.20. The activation energy, E$_a$ was found to decrease along with an increase in conductivity with increasing substitution concentration in BCTAK. Copyright © 2015 VBRI Press.

Keywords: Chemical synthesis; dielectric properties; electrical conductivity; ferroelectricity.

Prasanta Dhak received his Ph. D. degree from Jadavpur University, Kolkata in collaboration with Indian Institute of Technology Kharagpur, India in 2012. He currently holds a position of Postdoctoral Fellow in the Department of Materials Science and Engineering, Seoul National University, Republic of Korea. His research area is focused on nanomaterial science and solid state chemistry with special emphasis on ferroelectric, magnetic, ferromagnetic, photocatalytic, phosphor, fuel cell, solar cell and gas sensor. He is also interested in nanoparticle based drug delivery system, magnetic resonance imaging and magnetic hyperthermia.

Atreyee Kundu is a Ph.D student in the Department of Biological Sciences, Presidency University, Kolkata, India. She currently holds a position of Researcher in the Department of Plant Science, College of Agriculture and Life Science, Seoul National University, Republic of Korea. She is mainly interested in modern disciplines of plant genetic engineering, microbial biotechnology and molecular biology.

Debasis Dhak received his Ph. D. degree from Indian Institute of Technology Kharagpur, India in 2008. He joined as an Assistant Professor in Serampore College, Calcutta University in 2006 and then moved to the University of British Colombia, Canada as a postdoctoral fellow in 2008. Presently, he is working as an Assistant Professor in Sidho-Kanho-Birsha University, West Bengal, India since 2013. His research interest includes nanomaterials synthesis and characterizations in the area of ferroelectric, photocatalyst and acid catalysts etc. He is also interested in acid mist suppression and process improvement of industrial and synthetic zinc electrowinning.

Introduction

The ferroelectric properties of BaTiO$_3$ (BT) can be efficiently controlled by doping with different elements. It is possible to tailor the parameters such as maximum dielectric constant (ε$_m$), transition temperature (T$_C$), and dielectric diffuseness by suitable doping. Doping of either Ba-site ions or Ti-site ions modifies the T$_C$ and the nature of ferroelectric-paraelectric transition in BT. A-site doping

with cation can cause a decrease as well as an increase in T_C and a significant broadening of the transition is observed.

A good number of substituted BT compositions exhibit a diffuse phase transition; depart from the Curie-Weiss (CW) law, pronounced frequency dispersion, and the existence of spontaneous polarization well above and below the transition temperature namely, relaxor type behaviour. The observed departure from the CW law in such case is governed by the modified CW law [1] as given below:

$$\frac{1}{\varepsilon} - \frac{1}{\varepsilon_m} = \frac{(T - T_m)^\gamma}{C} \qquad (1)$$

In Eq. (1), C and γ are constants, and ε_m is the maximum dielectric constant at transition temperature T_{max}. In doped systems, unlike a well-defined and sharp T_C for the case of pure $BaTiO_3$, the transition is a diffuse one as it happens over a range of temperature. The temperature T_{max} is therefore defined as the temperature where the dielectric peak occurs. The constant, γ determined the diffusivity of the sample system. It varies between 1 and 2. In a limiting case, for a ferroelectric material, $\gamma = 1$ and the system behave accordingly with CW law. The constants γ and C are independent and change in accordance with each other in a reasonable manner in order to keep the ratio (T-$T_{max})^\gamma$/C constant.

The diffusive nature of the transition is attributed to inter- and intra-molecular strains. The inhomogeneous distribution of cations in the materials would also lead to diffuse phase transition (DPT) phenomenon [2-4]. Bobade et al., have studied the La- and Al-substitution in $BaTiO_3$ at A- and B- site, respectively [5]. The diffuseness increases with increasing substitution concentration, suggested the existence of polar nanodomains over a wide range of temperature, which is responsible for breaking long-range ordering and giving rise to a diffused phase transition. The increase in diffusivity is not followed by an increase in frequency dispersion, the reason being that there exists enough interaction among polar nanodomains so as to suppress frequency dispersion.

Ageing effect of ferroelectricity in Al doped and Ga doped $BaTiO_3$ was studied by Guo et al. [6]. The Al^{3+}-doping resulted in the lattice shrinkage since Al^{3+} (ionic radius $r \sim 0.0535$ nm) is smaller than Ti^{4+} ($r \sim 0.0605$ nm), and meanwhile oxygen vacancies are created to satisfy the requirement of the charge neutrality. Ga^{3+} ions ($r \sim 0.062$ nm), generated oxygen vacancies without lattice shrinkage [7]. The lattice shrinkage in Al^{3+} doped $BaTiO_3$ hindered the oxygen vacancies migration and hence suppressed the ageing effect on the ferroelectric behaviour.

Recently, Jahn-Teller distortion was proposed to be the common driving force for the cubic–hexagonal transition. Jahn-Teller distortion is caused by Ti_{Ti}^{3+} ions in the undoped material [8], or e.g., by Mn_{Ti}^{3+} To investigate this proposal, it appears to be useful to test also other Jahn-Teller active 3d transition elements. Like Mn_{Ti}^{3+}, also Cu_{Ti}^{2+} with its electron configurations d^9 exhibits a strong Jahn-Teller effect (JTE). However, to our knowledge, little is known about the occurrence of h-BT due to Cu-doping. Recently, Langhammer et al. have obtained first evidence that h-BT is produced by doping with 2 mol% Cu [8-10],

where it has been suggested that tetragonal and hexagonal phase coexist at room temperature for higher concentration of Cu substitution. The portion of tetragonal phase decreases with copper concentration, leading to a decrease and broadening of the dielectric anomaly at the Curie temperature. Dhak et al. also have shown that the diffuseness increased with an increase in the level of substitution in $BaTi_{1-3x}Cu_xNb_{2x}O_3$, which was evident from a corresponding increase in deviation from CW law [11]. This suggested the existence of polar nanodomain over a wide range of temperature, which was responsible for breaking long-range ordering and giving rise to a diffused phase transition.

The system investigated in this work, is $Ba_{1-x}Cu_xTi_{1-x}(AlK)_xO_3$. We have attempted to maintain the charge and site balance so as to avoid the formation of vacancies on either of the Ba or Ti sites. Here, a preliminary study of simultaneous substitution of Ba and Ti site in $BaTiO_3$ by Cu and Al-K respectively is reported, which shows very interesting ferroelectric behavior. It is known that as long as the A/B ratio stays between 0.98 and 0.99, the perovskite structure remains stable. All the compositions studied in this work fall within this tolerance limit. We report here on the synthesis, as well as the structure and dielectric property correlations.

Experimental

Powders of $Ba_{1-x}Cu_xTi_{1-x}(AlK)_xO_3$ (BCTAK) (where x = 0.05, 0.10, 0.15 and 0.20) were prepared by aqueous based chemical method [12-14], using high purity raw materials: $Ba(NO_3)_2$, (MERCK, Germany, GR grade) (99%), $Cu(NO_3)_2$, (MERCK, Germany, GR grade), $Al(NO_3)_3$, (MERCK, Germany, GR grade), $K(NO)_3$, (MERCK, Germany, GR grade), TiO_2, (Sigma Aldrich, 99.99%), Tartaric acid (Quest Chemicals, Kolkata, India (99%), TEA (triethanolamine) (SRL, Mumbai, India (97%)), HNO_3 (65%) (MERCK, Mumbai, India, GR grade) and NH_4OH (25%) (MERCK, Mumbai, India, GR grade). Initially powder produced by this process was nanosized. A flow chart of steps involved is provided in **Fig. 1**.
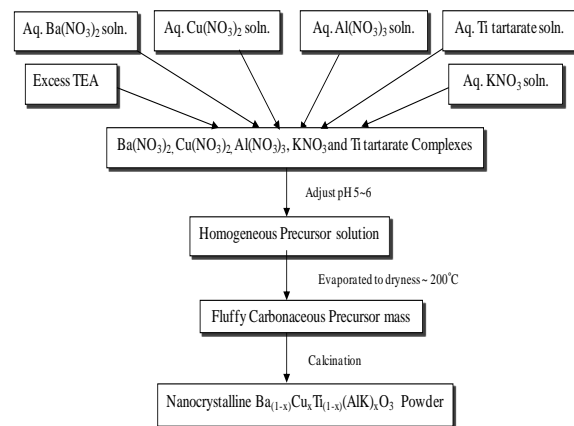

Fig. 1. Schematic representation of the precursor solution method for the synthesis of $Ba_{(1-x)}Cu_xTi_{(1-x)}(AlK)_xO_3$ where, x = 0.05, 0.10, 0.15, 0.20 powders.

For the synthesis of nanosized BCTAK ceramic powders, appropriate volumes of $Ba(NO_3)_2$, $Cu(NO_3)_2$,

Al(NO$_3$)$_3$, KNO$_3$ and Ti-tartarate were taken from their respective stock solutions, in accordance with the desired stoichiometry, and mixed together in a beaker of sufficient capacity. Commercially unavailable titanium tartarate was prepared from TiO$_2$ which was described by Dhak et al. [15]. The precursor solution was subsequently obtained by adding excess TEA (3 mol ratio with respect to per mol of the total metal ions) to avoid any chance of precipitation of the metal ions from the precursor solution. The polydented complexing/chelating agent TEA used, played a dual role by helping in the distribution of cations in the precursor solution throughout the TEA network so that the selective precipitation is prevented during the evaporation process and also aided in the formation of the fluffy, voluminous, mesoporous carbon rich precursor materials by heating at ~200°C. The materials provided heat by combustion during pyrolysis and facilitated the reduction of the external temperatures required for the desired phase formation.

Thermal analysis [differential thermal analysis (DTA) and thermal gravitometric analysis (TGA)] (Model DT-40, Shimadzu Co, Japan) of the voluminous mass was carried out to find the optimum formation temperature, in static air at a heating rate of 10°C/ min up to 1000°C, using alumina crucible. The black fluffy precursor mass after calcination at 700ºC for 2h, was characterized by X-ray diffraction at room temperature using Philips PW1710 X-ray diffractometer, equipped with a vertical goniometer and CuKα radiation source of wavelength (λ=1.514 Å). Measurement was performed at room temperature under vacuum to minimize air scatter. The XRD spectrum of Si crystal was used as a standard to calibrate the scanning angles. The data were collected over the 2θ angle range of $20° \leq 2\theta \leq 80°$. The step size of the scan was 0.04° 2θ, with a scanning speed of 0.02° 2θ/ s. The crystallite size of the material was calculated using Scherrer's equation [16, 17], $D = 0.89\lambda/\beta_{1/2}\cos\theta$, where, $\beta_{1/2}$ = half-peak width. In the calculation of crystallite size some errors arised due to strain effect and instrumental error. The instrumental errors were minimized by making the correction in the half-peak width (β) term [$\beta^2 = \beta^2$ (material) - β^2 (standard sample)]. Transmission electron microscopy (TEM) of the synthesized powder was carried out to study the microstructure and shape using JEM 2100 microscope using a LaB$_6$ filament operated at 200 kV. The sample was prepared by sonnicating a pinch of the powder for half an hour using acetone as dispersing solvent and then taken on a carbon coated (50 nm thickness) copper grid of 300 mesh. The calcined powders were then pressed into cylindrical pellets of 10 mm diameter and 2 mm of thickness, using a hydraulic press at a pressure of 190 MPa / cm^2. Polyvinyl alcohol (PVA) was used as a binder to reduce the brittleness of the pellet, which was burnt out during the high temperature sintering. The pellets were sintered at 900°C for 4 h in static air atmosphere. The surfaces of sintered pellets were gold coated (thickness 40 Å) by a sputtering technique to check the morphology by field emission scanning electron microscope (FESEM) using JEOLJSM 5800 at 20 kV at room temperature. To study the electrical properties of the material, both the flat surfaces of sintered pellet were polished and electroded with conducting high purity silver paint. The silver painted samples were dried at 200°C for 2 h to remove the

moisture, if any and then cooled to room temperature before taking electrical measurements. The dielectric and impedance parameters were obtained using a computer controlled impedance analyzer (HIOKI LCR HITESTER) at an ac signal of 1.0 V in a wide frequency range (10^2-10^6 Hz) at different temperatures (25-600°C). The polarization electric field (P-E) measurement was performed by polling the pellet at room temperature in a silicon oil bath under the DC field of 15 kV/cm for 1 h using APLAB high voltage DC power supply.

Results and discussion

Thermal analyses

Thermal characterization technique was used to find the optimum formation temperature for the compound. The thermogravimetric (TG) data and the corresponding derivative thermogravimetric (DTA) curve for representative precursor samples are shown from room temperature to 1000°C at the heating rate of 10°C/min in **Fig. 2**. From the DTA plot, a broad exothermic peak from 220°C to 600°C was observed which could be assigned due to the oxidation of carbonaceous remains from the decomposed metal-complexes and TEA. The TG plots showed a sharp and single-step weight loss in the temperature range of 220 to 600°C and no further weight loss after 600°C temperature was observed. The sharp and single step weight loss in this temperature range may be due to the evolution of various gases like CO, CO$_2$, NH$_3$, water vapor etc. during oxidation of the precursor by thermal effect. Above 700°C, there were no significant thermal effects observed in DTA curve and the corresponding TG curve showed no weight loss, implying the complete volatilization of carbon compounds.
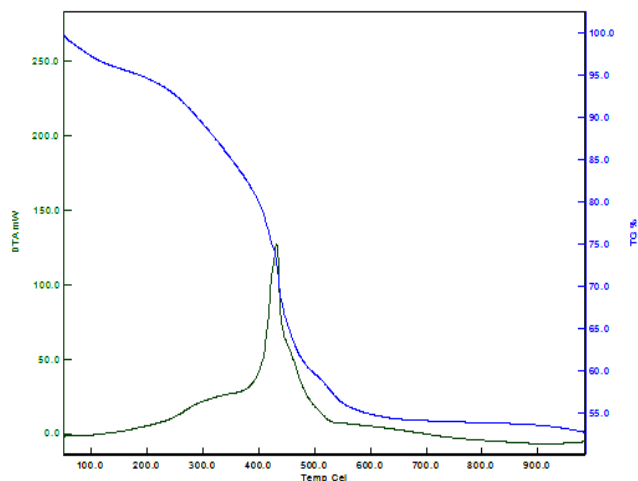

Fig. 2. DTA/TGA graph of Ba$_{0.8}$Cu$_{0.2}$Ti$_{0.8}$(AlK)$_{0.2}$O$_3$ black fluffy.

Structure and microstructure

Room temperature XRD studies of all the calcined powders were carried out to confirm the phase formation of the composition range studied for Ba$_{1-x}$Cu$_x$Ti$_{1-x}$(AlK)$_x$O$_3$ x = 0.05, 0.10, 0.15, 0.20 as shown in **Fig. 3 (a-d)**. Careful analysis of the X-ray data for all the compositions, between x = 0.05 and 0.20, appear to exhibit a single phase. The

elemental analyses (Energy dispersive X-ray) were also performed for all the compositions which showed satisfactory results as shown for BCTAK-0.05 in Fig. 3(inset) as representative one. The XRD peaks were indexed and the lattice parameters were determined in various crystal systems and configuration using a JCPDS data file. On the basis of the best agreement between observed and calculated d, i.e., $\sum d_{obs} - \sum d_{cal}$ = minimum, a tetragonal system was selected with JCPDS data file No. 83-1880 with space group P4/mmm. The lattice parameters, unit cell volume as well as the degree of tetragonality (c/a) are shown in **Fig. 4**.
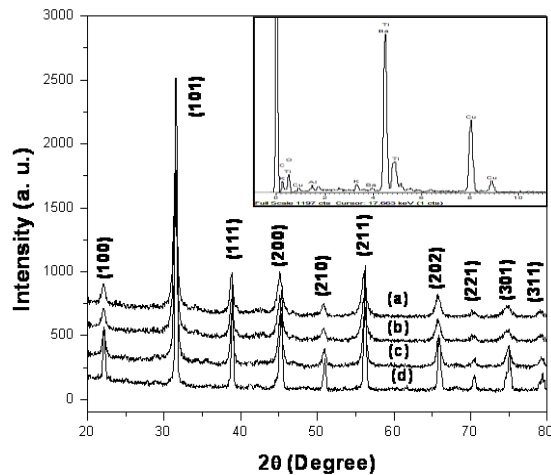
Fig. 3. XRD pattern of $Ba_{(1-x)}Cu_xTi_{(1-x)}(AlK)_xO_3$ ceramic powders calcined at 700ºC for 2h [(a) x = 0.05, (b) x = 0.10, (c) x = 0.15 and (d) x = 0.20] and EDX of $Ba_{0.95}Cu_{0.05}Ti_{0.95}(AlK)_{0.05}O_3$ powder.
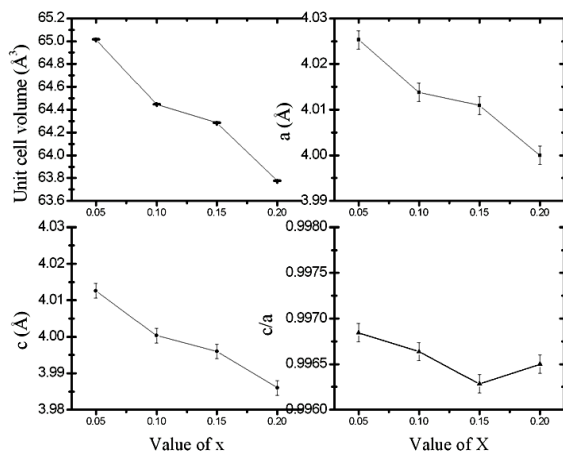
Fig. 4. Plot of (a) unit cell volume (b), (c) lattice parameters and (d) tetragonality as a function of substitution concentration (x) of BCTAK ceramics.

It is interesting to note that the c/a values were observed to be less than unity for all the studied materials though most of the reported substituted perovskite materials exhibited c/a values higher than unity [5, 11, 18]. However, Lahmar et al. have reported c/a value 0.997 for $BiFeO_3$ doped $LaMnO_3$ ferroelectric thin films at 2% doping level [19]. It could be clearly concluded that the extent of tetragonality [**Fig. 4 (d)**] as well as the unit cell volume [**Fig. 4 (a)**], decreased with increasing substitution concentration which was assumed to have reduced

dielectric constant [10]. The crystallite sizes, calculated using Scherrer's equation, are summarized in **Table 1**. The largest crystallite size 27 nm was observed to be at BCTAK x= 0.20.
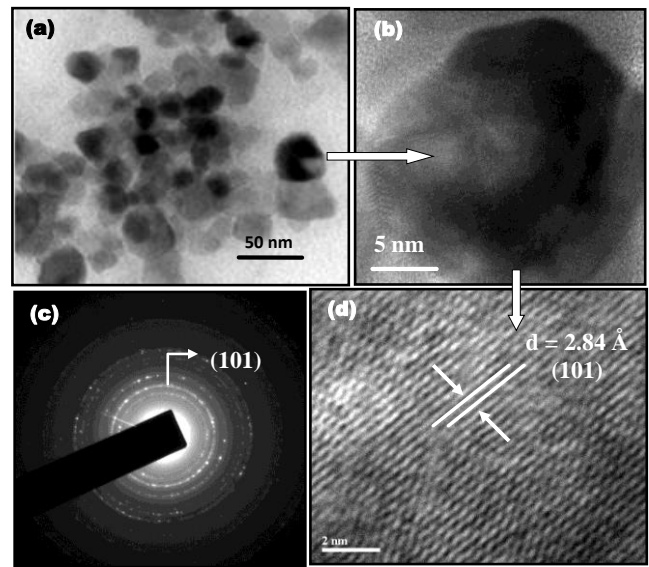

Fig. 5. (a) Bright field transimission electron microghaph, (b) selected area of particle, (c) SAED pattern of the selected particle and (d) high resolution TEM of $Ba_{0.8}Cu_{0.2}Ti_{0.8}(AlK)_{0.2}O_3$ powder.

Table 1. Comparisons of crystallite size, particle size, grain size, relative density, curie temperature, dielectric constant at curie temperature and dielectric loss at curie temperature of BCTAK (x = 0.05, 0.10, 0.15, 0.20) compositions.

$Ba_{1-x}Cu_xTi_{1-x}(AlK)_xO_3$	Crystallite Size (D) (nm)	Particle Size (P) (nm)	Grain Size (μm)	Density (%)	Curie Temperature (T_C) at 10 kHz	ε' at (T_C) (10 kHz)	tanδ at T_C (10 kHz)
X = 0.05	17	21	2	94	105	4218	0.085
X = 0.10	20	26	2.5	95	100	1183	0.017
X = 0.15	24	27.5	3.7	96	100	2404	0.075
X = 0.20	27	30	3.6	96	95	1953	0.070

A representative bright field TEM for BCTAK $x = 0.20$ is shown in **Fig. 5(a)** after calcinations of the precursor powders at their phase formation temperature 700°C for 2h. The bright field TEM micrograph represented the basic powder morphology in the sample, where the smallest visible isolated spot can be identified with particle/crystallite agglomerates. From the TEM study of the BCTAK powders, it was observed that the particles have an almost-spherical morphology. The average particle diameters calculated using UTI image tool software (version 3.0) ranges between 21 to 30 nm, which are summarized in **Table 1**, and are in close agreement with the crystallite size obtained from XRD after corrections. **Fig. 5(b)** shows a single, distinct, almost spherical nanoparticle of $Ba_{0.8}Cu_{0.2}Ti_{0.8}(AlK)_{0.2}O_3$ composition whereas **Fig. 5(d)** shows the corresponding high resolution transmission electron microscopy (HRTEM). From the HRTEM image we could notice a well-defined lattice fringes indicating a good level of crystallinity present in the nanopowder. The lattice spacing of the particle was found to be 2.84 Å, which corresponds to (101) plane of tetragonal phase of this materials. The corresponding selected area electron

diffraction (SAED) pattern was recorded from the same region of the sample as shown in **Fig. 5(c)**. It demonstrated distinct rings which again indicated the presence of polycrystalline nature of the sample. From the SAED patterns, the calculated lattice planes confirmed the presence of (101) plane of tetragonal structure of $Ba_{0.8}Cu_{0.2}Ti_{0.8}(AlK)_{0.2}O_3$. The individual plane identified from the SAED pattern correlated well with that of the HRTEM and XRD pattern.

The microstructures of the sintered pellets are shown in **Fig. 6(a-d)**. Usually grain growth takes place during sintering, which occurs both in porous and dense polycrystalline solids at high temperature. The equation for grain growth at a fixed temperature is given by:

$$G^m - G(0)^m = Kt, \qquad (2)$$

where G is the average grain size, $G(0)$ is the average size at $t = 0$, and K is a constant [20]. In case of ceramics, the value of m is often taken as 3. Usually the grain growth is inhibited in nanomaterials due to open porosity, grain growth inhibitors, and grain boundary segregation. Thus during sintering the size of the particle does not increase much. The grains separated by well-defined grain boundaries are visible. The average grain sizes of the sintered samples were found to be in the range between 2.0 and 3.7 μm. The grain sizes calculated from the micrographs using UTI image tool software (version 2.0) are summarized in Table I for all the samples. Table 1 also summarizes the relative densities obtained after sintering of the sample at $900°C$ for 4 h. Xylene was used as the liquid solvent (density = 0.87 g/cm^3) to measure the experimental density using the Archimedes method. A maximum of 96.5% relative density was achieved for BCTAK, $x = 0.15$. The effective improvement of densification may be due to the increase of the concentration of Cu^{+2} as reported earlier by Lin et al. [21].
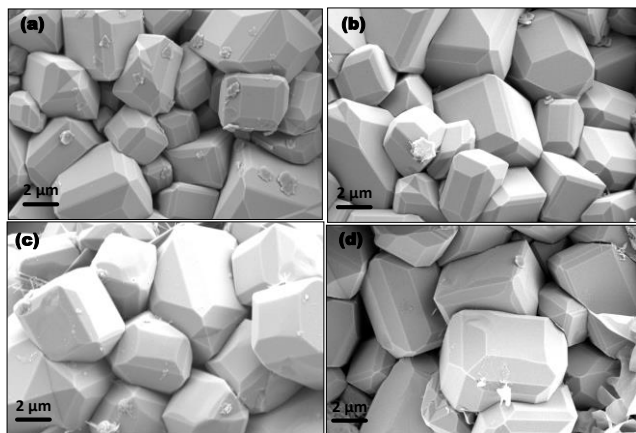

Fig. 6. Field emission scanning electron microscopy (FESEM) of of $Ba_{(1-x)}Cu_xTi_{(1-x)}(AlK)_xO_3$ ceramic powders [(a) x = 0.05, (b) x = 0.10, (c) x = 0.15 and (d) x = 0.20].

Dielectric properties

Temperature dependence of dielectric behavior at different frequencies (1 kHz, 10 kHz, 100 kHz and 1 MHz) for all the compositions of BCTAK is shown in **Fig. 7(a-d)**. The change in the transition temperature with frequency was not observed even for higher substitution concentrations of Cu^{2+}, Al^{3+}, and K^+ within the experimental span of frequency, which concludes the absence of any relaxor-type behavior. The values of the dielectric constant at and T_C for a fixed frequency of 10 kHz have been listed in **Table 1**. A relatively sharp dielectric peak at $T_C = 105°C$ with no frequency dispersion, similar to pure $BaTiO_3$, was observed for x = 0.05 composition. As x values increase to 0.10, 0.15 and 0.20, the dielectric peak gradually become broadened and diffused to a long temperature range called diffused phase transition. The steep increase in dielectric constant at low frequency is ascribed to space polarization. In particular, the effect of space polarization was prominently observed for the compositions BCTAK for $x = 0.15$ and x = 0.20. For BCTAK $x = 0.20$, a second order ferroelectric transitions was observed within this temperature range. Yu et al. have reported that coupled substitutions of Bi^{3+} for Ba^{2+} on the A site and Al^{3+} for Ti^{4+} on the B site would lead to a diffused phase transition with increasing substitution concentration [22]. Substitution of $BaTiO_3$ by $CuNb_2O_6$ substantially increased the dielectric diffuseness as reported by Dhak et al. [11].
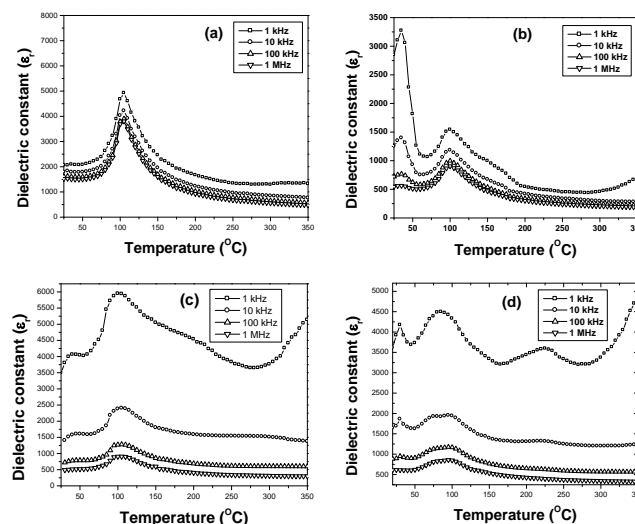

Fig. 7. Temperature dependence of dielectric constant for $Ba_{1-x}Cu_xTi_{1-x}(AlK)_xO_3$ ceramics with different frequency [(a) x = 0.05, (b) x = 0.10, (c) x = 0.15 and (d) x = 0.20].

It was also found that the T_C values (measured at 10 kHz) decreased with increasing doping concentrations as shown in **Table 1**. This shifting of T_C towards lower temperature with increasing x value could be attributed to the increased compositional disorderedness in the polar region [22, 23]. Due to the increasing level of substitution concentration, the ferroelectric long range order is disrupted causing an increase of compositional disorder and decrease of "average" Curie temperature. Furthermore, the increasing compositional disorder also results in a decrease of the dielectric maximaum. As listed in **Table 1**, the maximum dielectric constant at T_C, $\varepsilon_m = 4218$ was found to be maximum at BCTAK, x = 0.05 and rest of the compositions followed a decreasing trend as has been presumed and discussed in earlier section (Sec IIIB). However, lowest value of $\varepsilon_m = 1183$ was observed for BCTAK, x = 0.10. The substitution of Ti^{4+} ($R_{Ti}^{4+} = 0.75Å$)

by Al^{3+} ($R_{Al}{}^{3+}$ = 0.54 Å) and K^+($R_K{}^+$ = 1.64 Å) and Ba^{2+} ($R_{Ba}{}^{2+}$ = 1.61 Å) by Cu^{2+} ($R_{Cu}{}^{2+}$ = 0.73 Å) [7, 11, 24] ions resulted to a decreased unit cell volume and decreased tetragonality as shown in **Fig. 4 (a)** and **Fig. 4 (d)** respectively played an important role for decreasing both ε_m values as well as the T_C values [10]. The tangent losses for all the compositions were found to be in the range of 10^{-2} as listed in **Table 1**. The loss was found to be decreased with increasing substitution concentration. The minimum loss was observed for BCTAK, x = 0.10.
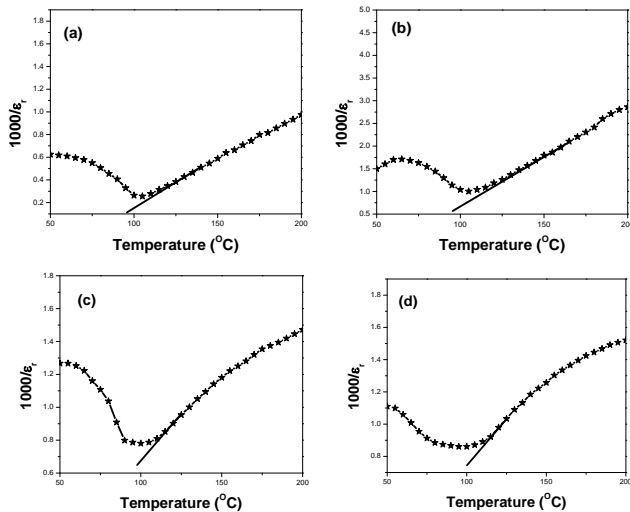
Fig. 8. Temperature dependence of the reciprocal of dielectric constant ($1/\varepsilon_r$) for $Ba_{1-x}Cu_xTi_{1-x}(AlK)_xO_3$ ceramics at 100 kHz [(a) x = 0.05, (b) x = 0.10, (c) x = 0.15 and (d) x = 0.20].

For the compositions investigated in this work, the Curie-Weiss law was not obeyed; the plot between $1000/\varepsilon$ and temperature (T) deviates from linearity. The deviation from the linearity at 100 kHz has been exhibited in **Fig. 8 (a-d)**, respectively, for the composition BCTAK, *x* = 0.05, 0.10, 0.15 and 0.20. These deviations from linearity aroused due to the diffused phase transitions (DPT) of the investigated compositions. The degree of diffuseness was calculated from the Currie-Weiss law from the plot $\ln(1/\varepsilon -1/\varepsilon_{max})$ vs $\ln(T-T_{max})$. If γ is equal to 2, a material will be a completely disordered ferroelectric having a DPT behavior. The dielectric data have been fitted to the modified CW law [Eq.(1). A plot of $\ln(1/\varepsilon -1/\varepsilon_{max})$ vs $\ln(T-T_{max})$ at 100 kHz at temperatures greater than T_C is shown in **Fig. 9**, and the constant γ, extracted from the slope is plotted as shown in **Fig. 9** (inset).

The constant γ that governs the diffuseness of transition increased from 1.22 at a doping level of *x* = 0.05 to 1.91 at the doping level of x = 0.2. The broadness of the peak is an indication of the disorder existing both on Ba^{2+} site and the Ti-site positions, which make the nanoregion of inhomogeneous composition in the specimens, compared with undoped BT. When Ti^{4+} sites are substituted by $Al^{3+}(R_{Al}{}^{3+}<R_{Ti}{}^{4+})$ and $K^+(R_K{}^+>R_{Ti}{}^{4+})$ ions and Ba^{2+} sites by Cu^{2+} ion ($R_{Cu}{}^{2+}<R_{Ba}{}^{2+}$), each substitution gives a different effect. The smaller ion in the case of both Cu^{2+} and Al^{3+} provide more space, which promote the ionic displacements. This would result in the mixing of various displacements of cations in the specimen and comprise

regions with different local Curie points T_C. The net effect exhibits a diffuse phase transition. The same effect was reported by Munpakdee et al. by partially substituting Ti^{4+} by Mg^{2+} and Nb^{5+} ions [25].
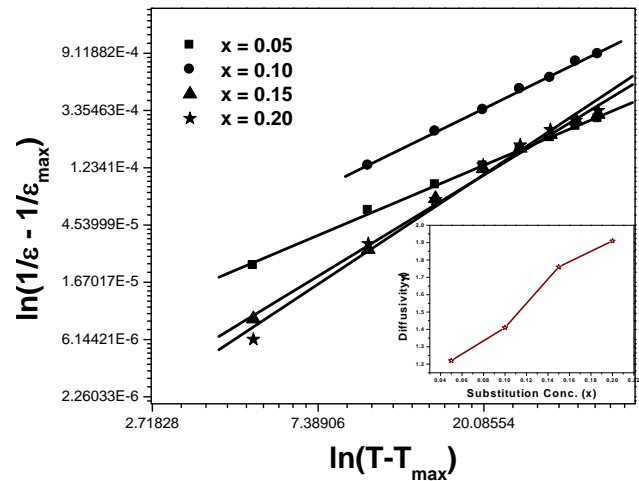

Fig. 9. Variation of $\ln(1/\varepsilon-1/\varepsilon_{max})$ with $\ln(T-Tmax)$ and variation of γ with doping concentration (inset) for $Ba_{1-x}Cu_xTi_{1-x}(AlK)_xO_3$ at 100 kHz [x = 0.05, 0.10, 0.15 and 0.20].

To establish the signature of feroelectricity in these materials, polarization-electric field (P-E) measurement was carried out for $Ba_{0.95}Cu_{0.05}Ti_{0.95}$ $(AlK)_{0.05}O_3$ at room temperature as shown in **Fig. 10**. From the P-E hysteresis loops of the studied material, a high value of saturation polarization (P_s = 19.24 $\mu C/cm^2$) and remnant polarization (P_r = 13.94 $\mu C/cm^2$) with a low coercive field of (E_c = 5.25 kV/cm) was observed. This large value of polarization in the studied materials may be due to the larger grain size in our composition, as the reversal polarization process of a ferroelectric domain is much easier inside a large grain than in a small grain [26].
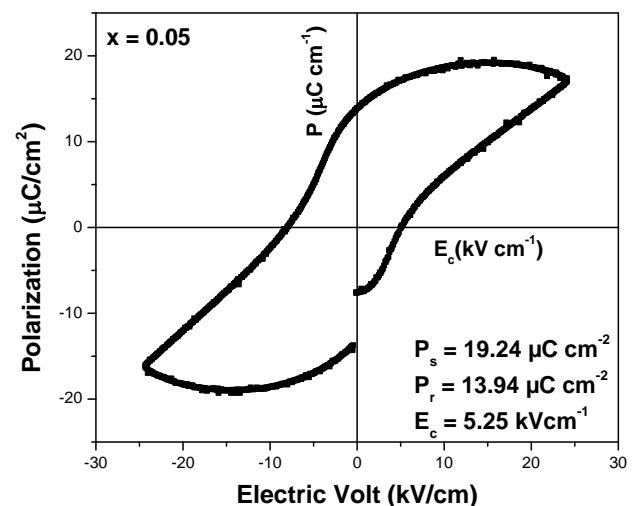

Fig. 10. Polarization vs electric field (P-E) hysteresis loop for the $Ba_{0.95}Cu_{0.05}Ti_{0.95}(AlK)_{0.05}O_3$ ceramics displayed at room temperature.

Electrical conductivity

DC conductivity: Electrical conduction in dielectrics is a thermally activated process, which arises due to the ordered
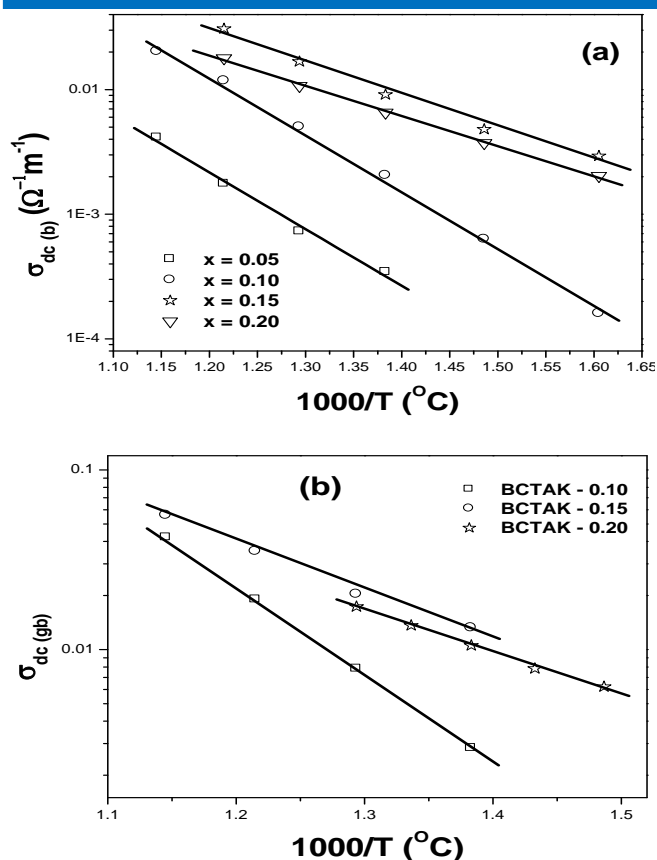
Fig. 11. Variation of DC conductivity with 10^3/T for (a) bulk and (b) grain boundary contribution.

motion of weakly bound charged particles under the influence of an electric field. Electrical conductivity is one of the significant property of the materials to be characterized depending on the nature of charge carriers that predominate the conduction process such as electrons/holes or cations/anions. The bulk conductivity of the compound at higher temperature were evaluated from the impedance data using the relation,

$$\sigma_{dc} = \frac{t}{R_b A}, \qquad (3)$$

where R_b is the bulk resistance, t is the thickness, and A is the area of the electrode deposited on the sample. This equation is also valid for grain boundary conductivity. The values of bulk resistance (R_b) and grain boundary resistance (R_{gb}) were obtained from the low frequency intercept of the semicircle on the real axis (Z') of the complex impedance plot (not shown here). **Fig. 11(a)** and **(b)** show the temperature variation of DC conductivity respectively for bulk and grain boundary i.e., σ_{dc} vs 10^3/T which follows the Arrhenius relation,

$$\sigma = \sigma_0 e^{\frac{-E_a}{kT}} \qquad (4)$$

where σ_o is a pre-exponential factor and E_a, k, and T are, respectively, the activation energy for conduction, Boltzmann's constant, and absolute temperature. Using this Arrhenius plot of dc conductivity, the corresponding activation energies for both grain and grain boundary conductivities were calculated from the slope of the linear

portion of the plot and the values are listed in **Table 2**. The activation energies (E_a) both for bulk and grain boundary conductivities were observed to be decreasing from 0.91 eV for BCTAK x = 0.05 to 0.48 eV for BCTAK x = 0.20. This observed decreasing tendency may be due to the marked effect of Jahn-Teller effect due to the presence of Cu^{2+} with a distortion of the lattice [27]. For high concentrations, the disorder increases by substitution, giving rise to a decrease in the activation energy E_a. In reduced crystals as the E_a decreases the conductivity increases with increasing substitution concentration as depicted in **Fig. 11 (a-b)**.

The value of activation energy for conduction clearly suggested a possibility that the conduction in the high temperature range was ionic in nature due to oxygen vacancies. In perovskite ferroelectric materials oxygen vacancies are considered one of the mobile charge carriers and mostly in titanates, ionization of oxygen vacancies creates conduction of electrons [28]. In our case, activation energy for grain boundaries was slightly more than the grain contribution that showed the resistive nature of the grain boundaries. The value of activation energy for grain and grain boundary gradually decrease with substitution concentration may due to Cu^{2+}, showing distribution of copper ions in both regions. The segregation of the substituent (mainly copper) at the grain boundaries is confirmed from scanning electron micrographs as shown in **Fig. 6**.

Table 2. Comparison of activation energy obtained from both bulk dc conductivity, grain boundary dc conductivity and ac conductivity of BCTAK (x = 0.05, 0.10, 0.15, 0.20) compositions.

$Ba_{1-x}Cu_xTi_{1-x}(AlK)_xO_3$	E_a from $\sigma_{dc(Bulk)}$ (eV)	E_a from $\sigma_{dc(Grain\ Boundary)}$ (eV)	E_a from σ_{ac} (eV)
X = 0.05	0.91	--	0.96
X = 0.10	0.90	0.98	0.93
X = 0.15	0.53	0.53	0.61
X = 0.20	0.48	0.49	0.52

AC conductivity: According to Jonscher, the origin of the frequency dependence of conductivity was due to the relaxation of ionic atmosphere after the movement of the particle. The variation of ac conductivity as a function of frequency (conductivity spectrum) at different temperatures is shown in **Fig. 12 (a-d)**.

Jonscher made an attempt to explain the behavior of ac conductivity using the following universal power law:

$$\sigma(\omega) = \sigma(0) + A\sigma\omega^n \qquad (5)$$

where σ_0 is a "dc" or frequency independent part, which is related to dc conductivity and the second term is of constant phase element (CPE) type. Making use of Jonscher's empirical expressions, Eq. (5) was rewritten as,

$$\sigma(\omega) = K\omega_p + K\omega_p^{1-n}\omega^n \qquad (6)$$

where p is the hopping frequency and K depends on the concentration of the mobile charge carriers. The high

temperature limiting value for *p* should be equal to the attempt frequency, which is independently accessible using IR spectroscopy [29].
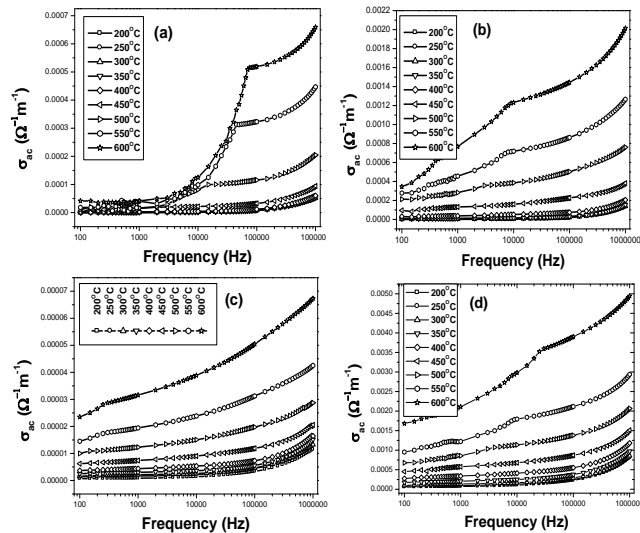

Fig. 12. Variation of ac conductivity with frequency at different temperature for $Ba_{1-x}Cu_xTi_{1-x}(AlK)_xO_3$ [(a) x = 0.05, (b) x = 0.10, (c) x = 0.15 and (d) x = 0.20].

The ac conductivity was calculated using a relation $\sigma_{ac} = \omega\varepsilon_r\varepsilon_o\tan\delta$. The curve in **Fig. 12(a-d)** shows dispersion, which shifts to the higher frequency side with a rise in temperature. The increasing trend of σ may be due to the disordering of cations between the neighboring sites and the presence of space charges that vanish at higher temperature and frequency. It is assumed that immediately after an ion hops to a new site (a new minimum in lattice potential energy) it is still displaced from the true minimum in potential energy, which includes a contribution from other mobile defects. At long time the defect could relax, until the true minimum coincides with the lattice site [29]. The ac activation energies calculated as summarized in **Table 2** are found to be a little bit higher than that of dc conductivity.

Conclusion

Nanocrystalline ceramic powder of $Ba_{1-x}Cu_xTi_{1-x}(AlK)_xO_3$ was synthesized by chemical route with an average particle size of 30 nm. On sintering maximum of 96.5% of relative density with average grain size of 3.7 μm was observed for BCTAK x = 0.15. Maximum dielectric constant (ε_m) was observed to be 4218 at T_C 105 °C at a frequency of 10 kHz. ε_m and T_C values were observed to be decreased on increasing x in BCTAK, may be due to the effect of disordering in the substituted ceramics caused mainly by Jahn-Teller effect due the presence of Cu^{2+}. The maximum diffusivity, γ = 1.91 was achieved for BCTAK x = 0.20. The diffuseness increases with an increase in the level of substitution, which was evident from a corresponding increase in deviation from CW law. This suggested the existence of polar nanodomain over a wide range of temperature, which was responsible for breaking long-range ordering and giving rise to diffused phase transition. The activation energy, E_a was found to decrease along with an increase in conductivity. The AC conductivity curve shows

dispersion, which shifts to the higher frequency side with a rise in temperature, may be due to the disordering of cations between the neighboring sites and the presence of space charges that vanish at higher temperature and frequency. P-E hysteresis study for BTCAK x = 0.05 showed a high value of saturation polarization (P_s = 19.24 $\mu C/cm^2$) and remnant polarization (P_r = 13.94 $\mu C/cm^2$), may be due to the larger grain size of the studied ceramics.

Reference

1. Suasmoro, S.; Pratapa, S.; Hartanto, D.; Setyoko, D.; Dani, U. M.; *J. Eur. Ceram. Soc.* **2000,** *20*, 309.
   DOI: 10.1016/S0955-2219(99)00143-0
2. Uchino, K.; Nomura, S.; *Integr. Ferroelectr.* 1982, *44,* 55.
   DOI: 10.1080/00150198208260644
3. Weill, F.; Rehspringer, J. L.; *J. Mater. Sci.* **1992,** *27,* 2316.
   DOI: 10.1007/BF01105037
4. Munpakdee, A.; Tontrakoon, J.; Siriwitayakorn, K.; Tunkasiri, T.; *J. Mater. Sci. Lett.* **2003**, *22*, 1307.
   DOI: 10.1023/A:1025714706703
5. Bobade, S. M.; Gulwade, D. D.; Kulkarni, A. R.; Gopalan, P.; *J. Appl. Phys.* **2005**, *97*, 074105.
   DOI: 10.1063/1.1879074
6. Guo, Y. Y.; Qin, M. H.; Wei, T.; Wang, K. F.; Liu, J. M.; *Appl. Phys. Lett.* **2010**, *97*, 112906.
   DOI: 10.1063/1.3490700
7. Shannon, R. D.; Acta Crystallogr. Sect. A: Found. Crystallogr. **1976**, *32*, 751.
   DOI: 10.1107/S0567739476001551
8. Langhammer, H. T.; Mueller, T.; Felgner, K. H.; Abicht, H. P.; *J. Am. Ceram. Soc.* **2000**, *83,* 605.
   DOI: 10.1111/j.1151-2916.2000.tb01239.x
9. Derling, S.; Muller, T.; Abicht, H. P.; Felgner, K. H.; Langhammer, H. T.; *J. Mater. Sci.* **2001,** *36*, 1425.
   DOI: 10.1023/A:1017532310071
10. Langhammer, H. T.; Mueller, T.; Boettcher, R.; Mueller, V.; Abicht, H. P.; *Journal of the European Ceramic Society*, **2004,** *24,* 1489.
    DOI: 10.1016/S0955-2219(03)00574-0
11. Dhak, D.; Dhak, P.; Ghorai, T. K.; Pramanik, P.; *J. Appl. Phys.* **2007**, *102*, 074117.
    DOI: 10.1063/1.2787149
12. Dhak, P.; Gayen, U. K.; Mishra, S.; Pramanik, P.; Roy, A.; *J. Appl. Phys.* **2009**, 106, 063721.
    DOI: 10.1063/1.3224866
13. Dhak, P.; Dhak, D.; Pramanik, K.; Pramanik, P.; *Solid State Sci.* **2008**, *10*, 1936.
    DOI: 10.1016/j.solidstatesciences.2008.04.019
14. Dhak, P.; Dhak, D.; Das, M.; Pramanik, K.; Pramanik, P.; *Mat. Sci. & Eng. B* **2009**, *154*, 165.
    DOI: 10.1016/j.mseb.2009.09.011
15. Dhak, D.; Pramanik, P.; *J. Am. Ceram. Soc.* **2006**, *8*, 1014.
    DOI: 10.1111/j.1551-2916.2005.00769.x
16. Cullity, B. D.; Stock, S. R.; Elements of X-Ray Diffraction, 3rd Edition, Pearson Education International, pp. 170.
17. Shukla, S.K.; Agorku, E.S.; Mittal, H.; Mishra, A.K.; *Chem. Pap.* **2014**, *68*, 217.
18. Kumada, N.; Ogiso, H.; Shiroki, K.; Wada, S.; Yonesaki, Y.; Takei, T.; Kinomura, N.; *Materials Letters* **2010**, *64*, 383.
    DOI: 10.1016/j.matlet.2009.11.021
19. Lahmar, A.; Habouti, S.; Solterbeck, C. H.; Souni, M. E.; Elouadi, B.; *J. Appl. Phys.* **2009**, *105*, 014111.
    DOI: 10.1063/1.3063813
20. Cullity, B. D.; Elements of X-Ray Diffraction (Addison-Wesley, Philippines), **1978,** pp. 284.
21. Lin, D.; Kwok, K. W.; Chan, H. L. W.; *J. Appl. Phys.* **2007,** *102,* 074113.
    DOI: 10.1063/1.2787164
22. Yu, H.; Ye, Z. G.; *J. Appl. Phys.* **2008** , *103*, 034114.

DOI: 10.1063/1.2838479

23. Bokov, A. A.; Rayevskii, I. P.; Smotrakov, V. G.; Prokopalo, O. I.; *Phys. Status Solidi A* **1986,** *93*, 411.
    DOI: 10.1002/pssa.2210930202
24. Jia, Y. Q.; *J. Solid State Chem.* **1991,** 95, 184.
    DOI: 10.1016/0022-4596(91)90388-X
25. Munpakdee, A.; Pengpat, K.; Tontrakoon, J.; Tunkasiri, T.; *Smart Mater. Struct.* **2006**, *15,* 1255.
    DOI: 10.1088/0964-1726/15/5/014
26. Leu, C.; Chen, C. Y.; Chien, C. H.; Chang, M. N.; *Appl. Phys. Lett.* **2003,** *82*, 3493.
    DOI: 10.1063/1.1576308
27. Ouedraogo, A.; Palm, K.; Chanussot, G.; *J. Scientific Research* **2009,** *1*, 192.
    DOI: 10.3329/jsr.v1i2.1876
28. *Kroger, F. A.; Vink, H. J.; Solid State Physics- Advances in Research and Applications* (New York: Academic) 1956, pp. - 307
    DOI: 10.1016/S0081-1947(08)60135-6
29. Raymond, O.; Font, R.; Suárez-Almodovar, N.; Portelles, J.; Siqueiros, J. M.; *J. Appl. Phys.* **2005,** *97*, 084107.
    DOI: 10.1063/1.1870099